Scaling and transport analyses based on an international edge turbulence database

P. Simon,[1, 2, a)] M. Ramisch,[1] A.A. Beletskii,[3] A. Dinklage,[4] M. Endler,[4] S. Marsen,[4] B. Nold,[1] U. Stroth,[2] P. Tamain,[5] and R. Wilcox[6]

[1)] *Institut für Grenzflächenverfahrenstechnik und Plasmatechnologie, Universität Stuttgart, 70569 Stuttgart, Germany*

[2)] *Max-Planck-Institut für Plasmaphysik, 85748 Garching, Germany*

[3)] *Institute of Plasma Physics, NSC Kharkov Institute of Physics and Technology, 61108 Kharkov, Ukraine*

[4)] *Max-Planck-Institut für Plasmaphysik, 17491 Greifswald, Germany*

[5)] *EURATOM/CCFE Fusion Association, Culham Science Centre, Abingdon, Oxon, OX14 3DB, UK*

[6)] *University of Wisconsin-Madison, Madison, Wisconsin 53706, USA*

(Dated: 30 May 2014)

Microscopic turbulence properties in the edge of toroidally confined fusion plasmas are studied by comparative analysis of experimental data from seven devices, collected in an international edge turbulence database (ETDB). The database contains Langmuir probe measurements of fluctuations in the floating potential and ion saturation current across the last closed flux surface (LCFS). They are used to address statistical properties and particle transport. Universal features of plasma edge turbulence such as an increase in skewness across the scrape-off layer (SOL) as footprints of density blobs are recovered in all devices. Analysis of the correlation lengths and times reveals power law scaling relations with macroscopic drift-wave parameters, albeit weaker than would be expected for drift-wave turbulence. As a result, the turbulent diffusivity scales with the inverse of the magnetic field strength, which is closer to Bohm-like scaling than to gyro-Bohm scaling. Nearly identical scaling relations are determined in the confined plasma edge and the SOL, pointing to a strong connection between drift-wave turbulence in the edge and blobs in the SOL. The contributions of blobs and holes (negative density spikes) to the radial particle transport are analyzed qualitatively with a conditional averaging approach. Blobs are connected to outward transport in the SOL of all devices whereas holes exhibit no uniform propagation pattern.

[a)] Author to whom correspondence should be addressed. Electronic mail: patrick.simon@ipp.mpg.de

I. INTRODUCTION

Anomalous transport through electrostatic fluctuations in the edge of magnetically confined fusion plasmas has been identified as a major contributor to particle and energy losses and is thus fundamentally responsible for the global confinement properties.[1,2] A corresponding global turbulent diffusivity can be deduced from mixing-length estimates for the purpose of scaling studies. These estimates are based on turbulence characteristics on a microscopic level, namely typical correlation lengths L_c and times τ_c. Theory for drift waves predicts that τ_c should grow proportional to the characteristic timescale $L_n/c_\mathrm{s} \propto L_n\sqrt{m_i/T_e}$.[3] m_i is the ion mass and T_e the electron temperature. The density scale length L_n characterizes the gradient of the plasma density n (or pressure p, at constant temperature): $L_n = n/\left|\nabla n\right|$. Similarly, L_c is expected to scale linearly with the drift scale $\rho_\mathrm{s} = \sqrt{T_e m_i}/(eB)$, where e refers to the elementary charge and B to the magnetic field strength.[4] There are many variations of drift-wave turbulence, and these scaling predictions are taken from a simple local slab model. Inserting these local drift-wave scaling relations for the microscopic parameters L_c and τ_c into the random-walk expression for the turbulent diffusivity yields the so-called gyro-Bohm scaling:

$$D \propto \frac{L_\mathrm{c}^2}{\tau_\mathrm{c}} \propto \frac{\rho_\mathrm{s}^2}{L_n/c_\mathrm{s}} = D_\mathrm{B}\frac{\rho_\mathrm{s}}{L_n} \propto \frac{1}{B^2} \tag{1}$$

The inverse dependence on B^2 suggests that turbulent transport might be limited effectively by increasing the magnetic field strength. The quantity D_B is called the Bohm diffusivity. It is proportional to $1/B$, thus turbulent transport is reduced less by increasing B if the diffusivity exhibits Bohm-like rather than gyro-Bohm-like scaling.

Langmuir probe data from seven fusion experiments, including stellarators and tokamaks, has recently been collected in a database[5] for systematic intermachine comparison of the characteristics of plasma edge turbulence. This article presents the first detailed statistical analysis of the database. The data allows the determination of the typical length and time scales to determine the transport scaling across the different experiments. Moreover, poloidal electric field measurements are available for the evaluation of the radial $E \times B$ dynamics of intermittent density structures. These so-called blobs have been detected in many fusion experiments[6–13] and play a crucial role in SOL transport. Here, the contribution of blobs (positive density spikes) and holes (negative spikes) to turbulent particle transport is studied

in the inner edge and the SOL. The focus on transport scaling on a microscopic level sets this work apart from previous comparative studies of plasma edge turbulence using Langmuir probes.[14–16]

This paper is organized as follows: Section II introduces the database. Since the database does not cover details on equilibrium profiles, microscopic turbulence characteristics in this work are opposed to macroscopic estimates of drift-wave parameters at the LCFS. In Sec. II, these estimates are also introduced and discussed. Section III outlines the main statistical analysis methods. The experimental results on universal features, transport scaling and blob dynamics are presented in Sec. IV and summarized in Sec. V.

II. THE EDGE TURBULENCE DATABASE

In order to investigate the turbulent behavior in various fusion devices, a platform was established to collect comparable experimental data from multiple experiments. This framework has been installed as part of the International Stellarator/Heliotron Profile Database (ISHPDB).[17] The goal of this international edge turbulence database (ETDB) is to allow easy access to turbulence measurement data for the purposes of inter-machine comparisons. As of March 2014, experimental data from the two tokamaks ASDEX Upgrade (AUG)[18] and MAST,[19] as well as the five stellarators HSX,[20] TJ-K,[21] Uragan-3M (U3M),[22] Wendelstein 7-AS (W7AS)[23] and WEGA[24] has been collected in the ETDB. There are two available datasets from W7AS and WEGA, taken at different magnetic field strengths.

The entries of the ETDB consist of measurements taken with Langmuir probes during L-mode discharges. They measure the floating potential Φ_{fl} and the ion saturation current I_{sat}. Assuming negligible temperature variations, the fluctuations $\tilde{\Phi}_{\mathrm{fl}}$ and $\tilde{I}_{\mathrm{sat}}$ of these quantities are directly proportional to the fluctuations of the plasma potential ($\tilde{\Phi}_{\mathrm{p}}$) and the plasma density ($\tilde{n}$), respectively.

The ETDB entries contain measurements from a minimum of three probe tips, arranged poloidally along the same flux surface, where the outer probes measure Φ_{fl} and the central probe I_{sat}. This setup allows the calculation of radial turbulent particle fluxes due to $\tilde{E}_\theta \times B$ drifts, where the fluctuations of the poloidal electric field ($\tilde{E}_\theta$) are estimated from the $\tilde{\Phi}_{\mathrm{fl}}$ measurements. The probes have to be radially mobile and should include measurements on both sides of the last closed flux surface (LCFS). All measurements at different radial

positions for one discharge (or a number of comparable discharges) are grouped into one dataset for the determination of radial profiles. Each data file contains the absolute radial position, the radial distance from the LCFS d_s, the poloidal distance of each probe tip from the magnetic midplane as well as their uncertainties.

Some general information is provided for each dataset. This contains the following device parameters and specifics about the discharge conditions: the major radius R, the minor radius a, the working gas, the safety factor q, the magnetic field strength B as well as its direction (clockwise or counter-clockwise, when seen from above) and the average plasma density n. Since the ETDB does not cover equilibrium profiles, it contains characteristic average values of the equilibrium measures in the vicinity of the LCFS. Despite the fact that usually there are two different gradient scale lengths L_n in the inner edge and the SOL, both L_n do not differ by an order of magnitude and the relative error to the average around the LCFS is even less than about 50%. Hence, the deviation from the approximate value, by which L_n is well represented here, is not decisive for scaling analyses separated in and outside the LCFS. Table I lists these parameters for all current ETDB datasets.

The values for q (except for q_{95} for tokamak plasmas), B, n as well as electron (T_e) and ion (T_i) temperatures are LCFS values, too. Macroscopic characteristic drift-wave parameters ρ_s and c_s are deduced from the values listed in Tab. I and used in scaling analyses. Usually, radial dependencies of the independent variables in the regression analyses should be taken into account if both sides of the LCFS are treated separately. Relative changes in B of the order of 1% in the observed radial ranges are of minor importance in the scaling studies, especially as compared to inter-machine variations. In contrast, radial T_e dependencies seem to be more crucial. Similar to L_n, T_e is over- or underestimated on each side of the LCFS, if only the LCFS average is used. Systematic over- or underestimation does not alter the result of the regression analysis. As an orientation, device to device discrepancies by a factor of 1.5 in the temperature under the square root, however, would correspond to a shift by the symbol size on the abscissa of following logarithmic representations. Even though previous studies[25] did not reveal a clear correlation between turbulence properties and local T_e, caution is needed when comparing local scaling results based on macroscopic parameters (as done in Sec. IV B).

Fluctuations in the plasma temperature have been shown to be negligible in low-

TABLE I. Number of radial measuring positions n_{pos}, LCFS distance d_{s} and average device and discharge parameters at the LCFS in the region of the probes. Negative sign in the B column indicates a counter-clockwise field direction.

Dataset	n_{pos}	d_{s} (mm)	R (m)	a (m)	q	B (T)	n (10^{18}/m^3)	T_e (eV)	T_i (eV)	L_n (mm)
AUG	10	−10...31	1.6	0.5	4	1.5	13	40	40	12.5
HSX	21	−12...24	1.49	0.07	0.89	−0.88	1	70	30	17
MAST	12	−13...70	0.85	0.65	10	0.35	4	20	30	22-35
TJ-K	13	−32..28	0.6	0.1	3	−0.044	0.2	8	1	56
U-3M	9	+5...25	1	0.12	3	−0.64	0.4	50	50	5
W7AS low B	37	−17...42	2	0.17	2.95	−1.27	5	80	80	23
W7AS high B	39	−17...51	2	0.17	2.95	−2.55	80	80	80	17
WEGA low B	30	−26...32	0.72	0.12	5	−0.055	0.2	12	1	33
WEGA high B	30	−31...12	0.72	0.12	5	−0.48	1	5	1	31

temperature plasmas like TJ-K.[26] However, recent results both from experiments at ASDEX Upgrade[27] as well as simulations for AUG edge parameters[27,28] indicate that in high-temperature plasmas, electric field and, therefore, turbulent transport approximations from Φ_{fl} measurements could suffer from the influence of temperature fluctuations. Since data on temperature fluctuations is not available in the database, the analyses presented here are based on the floating potential.

III. DATA ANALYSIS METHODS

A. Correlation functions

The basis for the determination of the correlation time τ_{c} and the correlation length L_{c} is the cross-correlation function. In its normalized form it is defined as

$$C_{XY}(\delta t) = \frac{1}{\sigma_X \sigma_Y} \int \tilde{X}(t)\tilde{Y}(t+\delta t)\mathrm{d}t \tag{2}$$

and takes values between -1 and 1. It describes the similarity between two series of data, $X(t)$ and $Y(t)$ with standard deviations σ_X and σ_Y, displaced by a time difference δt. The tilde notation refers to the mean-free fluctuations, i.e. $\tilde{X} = X - \langle X \rangle$, $\langle \tilde{X} \rangle = 0$.

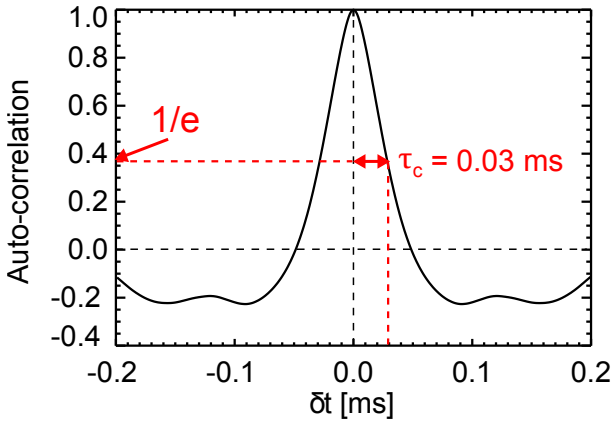

FIG. 1. Determination of τ_c from the I_{sat} auto-correlation function for a TJ-K measurement at the LCFS.

A special case of this function is the auto-correlation function $C_{XX}(\delta t)$, which compares a time series to itself. τ_c is calculated as the time lag at which the auto-correlation function of the I_{sat} measurement falls down to a value of $1/e$ (see Fig. 1). To estimate the accuracy of τ_c this procedure is done for multiple subsets of the given signal, which are then combined to an average result.

In principle, spatial correlation analyses require an adequate spatial resolution of the fluctuation signal. For the ETDB analysis, however, the sets usually only contain simultaneous measurements of Φ_{fl} at two locations, and I_{sat} at one. In order to calculate an estimate of L_c, an approximation has to be used: the zero-time-lag cross-correlation $C_{\Phi_1\Phi_2}$ between two Φ_{fl} measurements at different spatial distances can be used as an estimate of the spatial auto-correlation function. The peak of this auto-correlation function is expected to be Gaussian in shape,[29] where the width is given by the correlation length L_c. As the correlation is known for a single value of δl, L_c can be calculated:

$$L_c = \sqrt{-\delta l^2 / \log\left(C_{\Phi_1\Phi_2}\right)} \tag{3}$$

As for τ_c, the correlation length is calculated from several subsets of the data to obtain an average value and an estimate of its accuracy. Because of the estimation of L_c by direct calculation from a single point – instead of a fit to a number of points at different radial positions – the quantitative results should be interpreted with caution. They should, however, be in the correct order of magnitude, making them suitable for scaling analyses.

B. Conditional averaging

The conditional averaging method is a tool to separate the coherent component of a fluctuating signal from the random component.[30,31] Any fluctuation $\tilde{X}(t)$ that is measured in a parameter is partially due to random fluctuations $\tilde{X}_{\mathrm{r}}(t)$ and partially due to coherent events $\tilde{X}_{\mathrm{c}}(t)$, such as intermittent density bursts (known as blobs), which are observed in the scrape-off layer of fusion plasmas: $\tilde{X}(t) = \tilde{X}_{\mathrm{r}}(t) + \tilde{X}_{\mathrm{c}}(t)$.

Assuming that all intermittent events in a density signal are of similar shape, the average shape of a density burst can be extracted by conditional averaging. In order to detect coherent structures, the time series $\tilde{X}(t)$ is checked for a specified condition $\tilde{n} > \alpha\sigma_n$ in the amplitude. By choosing a trigger value larger than the standard deviation σ_n, the likelihood of falsely identifying random fluctuations as coherent events is reduced. This condition is used on the entire time series, resulting in a number of N identified events at times t_j, $j = 0, 1, ..., N-1$. In the next step, a segment $\tilde{X}(T_j)$ in the range $T_j \in [t_j - \tau, t_j + \tau]$ is extracted around every one of these points. The time τ is chosen large enough to easily cover typical blob lifetimes. Averaging over these segments results in the coherent part of the signal, while the random component cancels out.

IV. RESULTS

This section presents results from a wide variety of statistical analyses of the ETDB data.

A. Basic statistical properties

In order to detect principal similarities in plasma edge fluctuations, the basic statistical and spectral properties are examined. Figure 2 shows the auto-power spectra for all ETDB devices. From each device, one I_{sat} time series entry from a location near the LCFS was taken. In the cases of WEGA and W7AS, an entry from the low-B dataset was taken. Each power spectrum has been normalized with its maximum value.

The spectra are generally found to be Kolmogorov-like with a power-law decay over several decades in the high-frequency range. The spectral indices appear quite similar although the spectra have not been corrected for Doppler shifts from background rotation. Power spectra from various devices with similar behavior have been compared previously.[16] Some

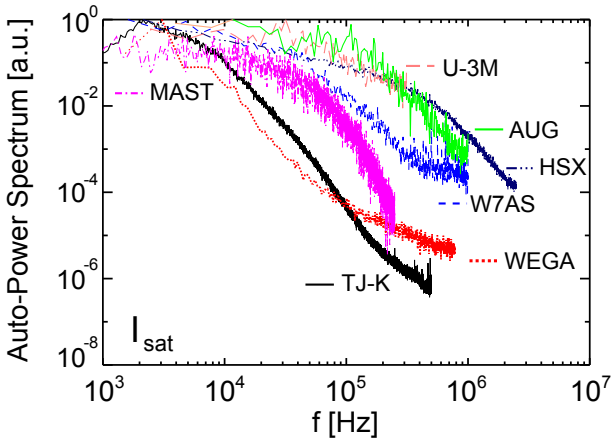

FIG. 2. Auto-power spectra of the $I_{\rm sat}$ measurements near the LCFS. The curves were normalized to their respective maximum value (WEGA and W7AS data low-B datasets).

spectra, e.g. from TJ-K and HSX, suggest a second inertial range at lower frequencies as characteristic for turbulence of two-dimensional nature. The frequency $f_{\rm bend}$ at which there is a bend in the spectrum and the steep inertial range begins is different for the devices and tends to smaller values for lower temperatures (TJ-K, WEGA, MAST).

In Fig. 3 $f_{\rm bend}$ is plotted over the characteristic frequency $v_{\rm dia}/\rho_{\rm s}$. $v_{\rm dia}$ is the electron diamagnetic velocity:

$$v_{\rm dia} = \frac{|\nabla p_e|}{enB} \approx \frac{T_e}{eL_nB} \Rightarrow \frac{v_{\rm dia}}{\rho_{\rm s}} \approx \frac{c_{\rm s}}{L_n} \tag{4}$$

The plot suggests a nearly linear dependence of the bend frequency on this characteristic quantity. In fact, a nonlinear regression analysis with $f_{\rm bend} \propto (v_{\rm dia}/\rho_s)^\alpha$ reveals an exponent $\alpha = 0.9 \pm 0.1$, i.e. a linear dependence within the uncertainty. The uncertainty is mostly attributed to the U-3M data point, which can be regarded as an outlier: a weak bend is detected at about 40 kHz in the power spectrum (Fig. 2), but it may be possible that a more clear bend would be detected at a frequency higher than the Nyquist frequency of the present dataset.

A consequence of the linear dependence is a relatively constant product of the drift scale $\rho_{\rm s}$ and the bend wavenumber $k_{\rm bend} \propto 2\pi f_{\rm bend}/v_{\rm dia}$ (i.e. $1/k_{\rm bend} \propto \rho_{\rm s}$), as pictured in Fig. 4. The result of a corresponding regression analysis does not seem to be conclusive because of the large relative uncertainty of the exponent. If, however, the U-3M dataset is disregarded as an outlier, the values of $k_{\rm bend}\rho_s$ vary only slightly, within 0.1 to 0.3, in the range of $k_{\rm bend}$

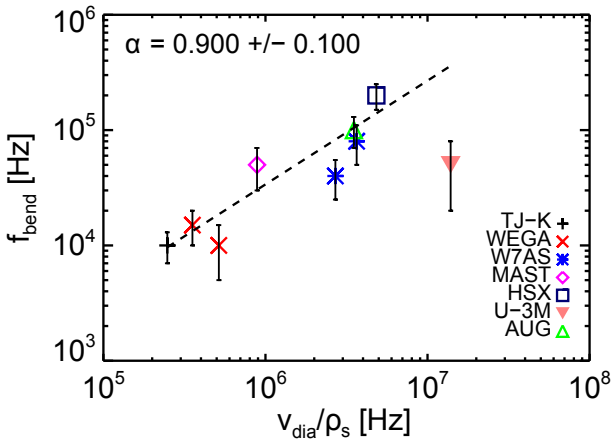

FIG. 3. Scaling of the bend frequency with the characteristic quantities v_{dia} and ρ_{s}. The dashed line shows the best power law fit for $f_{\mathrm{bend}} \propto (v_{\mathrm{dia}}/\rho_{\mathrm{s}})^{\alpha}$.

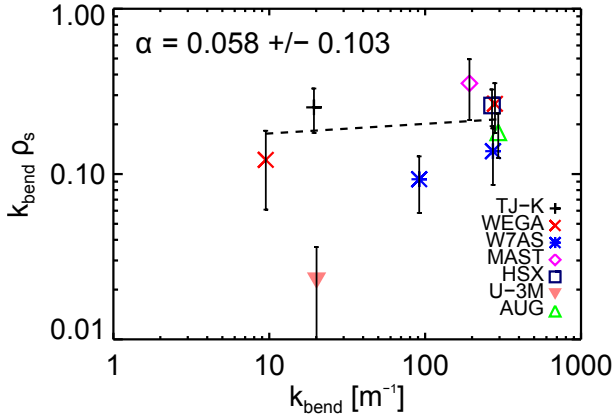

FIG. 4. Product of bend wavenumber k_{bend} and ρ_{s} for the ETDB devices with power law fit $k_{\mathrm{bend}}\rho_{\mathrm{s}} \propto k_{\mathrm{bend}}^{\alpha}$.

from about 10 to 300 m^{-1}. Therefore, $k_{\mathrm{bend}}\rho_s$ can be considered as reasonably constant.

In comparison with theory, linearly most unstable drift modes are expected at $k\rho_{\mathrm{s}} \approx 1$. Here, the linear ρ_{s} dependence of most unstable wavelengths shows up in the injection range of a typical 2D turbulence spectrum. This corresponds to previous results that show a constant product of average poloidal wavenumber and ρ_s.[14,32]

Further similarities of the ETDB sets can be found in the probability distribution functions (PDFs) of the fluctuations. Figure 5 shows the PDFs of I_{sat} measurements near the LCFS. The abscissa shows the fluctuation amplitude, expressed in multiples of the standard deviation σ_I. Almost all curves are close to a Gaussian distribution, i.e. nearly symmetrical

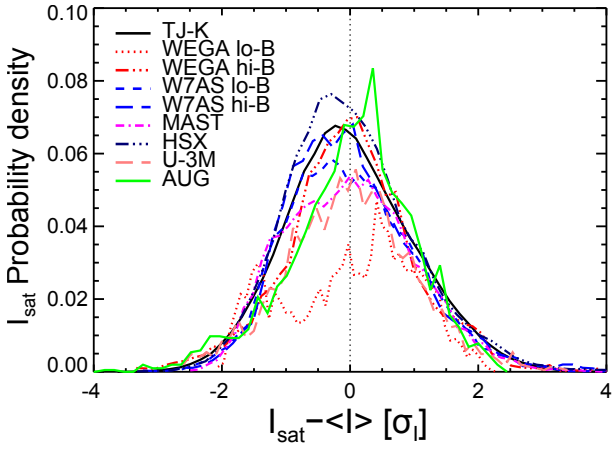

FIG. 5. PDF for near-LCFS measurements of $I_{\rm sat}$ in all ETDB datasets. PDFs are normalized to unity and plotted over the fluctuation from the mean value in multiples of the standard deviation.

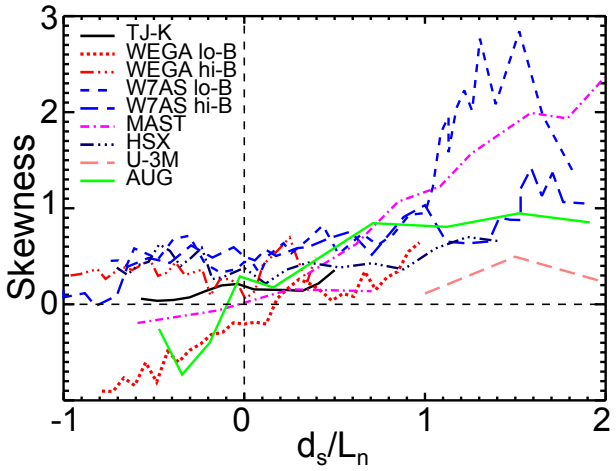

FIG. 6. Radial profiles of the $I_{\rm sat}$ skewness.

and falling off towards zero within 3 standard deviations. The strongest exception is found in the low-B set from WEGA, which has a negative skewness.

Figure 6 shows the radial profiles of the $I_{\rm sat}$ skewness around the LCFS. For a better comparison between all data, the radial position is given in terms of the distance from the LCFS $d_{\rm s}$ normalized to the density scale length L_n. As a general trend, the skewness increases beyond the LCFS in the scrape-off layer. In some cases (low-B WEGA, MAST and AUG) it changes sign from negative inside to positive outside the LCFS. This can be understood as a larger presence of intermittent positive density spikes (blobs) in the SOL region for all ETDB devices, while negative density spikes (holes) are more prevalent inside

the LCFS in some cases. These findings recover results of separate earlier studies of blobs in the ETDB devices[8,10–12] and are consistent with findings on universal properties of the PDF from other devices like the TCV tokamak.[33–36]

B. Scaling of turbulence properties

Turbulence in the plasma edge inside the LCFS is supposed to be dominated by drift-wave dynamics.[37] The database provides suitable information to test theoretical expectations for the scaling of correlation times (τ_c) and lengths (L_c) with L_n/c_s and ρ_s, respectively. The radial variation of τ_c and L_c – obtained from correlation analyses according to Sec. II – is found to be small. This justifies the use of the radial average to be compared to nominal values of L_n/c_s and ρ_s at the LCFS.

Figure 7 shows the analysis of the scaling relation between τ_c and L_n/c_s for the ETDB data. The error bars contain the spread of τ_c over the radial profile, as well as the uncertainty of every data point, which was obtained from calculating and averaging τ_c over multiple subsets.

The data shows a power law relation between τ_c and the quantity L_n/c_s, albeit with some scattering of the τ_c values. The best fit for the scaling exponent yields $\alpha = 0.53 \pm 0.04$. This is a weaker scaling relation than the predicted linear one, but it falls into a comparable range as results from previous scaling experiments on a single device.[25] To verify that the averaging over the entire radial profiles was acceptable, the analysis was repeated separately for the inside region ($-1 < d_\mathrm{s}/L_n < 0$) and the SOL region ($0 < d_\mathrm{s}/L_n < 2$) of the profiles. The resulting scaling exponents are $\alpha_\mathrm{in} = 0.60 \pm 0.04$ and $\alpha_\mathrm{SOL} = 0.52 \pm 0.04$, i.e. they are compatible with the average result. The observed scaling with respect to L_n is consistent with a prediction for ballooning-interchange turbulence that also incorporates the curvature radius R_c, namely $\tau_\mathrm{c} \propto \sqrt{R_\mathrm{c} L_n}/c_\mathrm{s}$.[38]

It must be stressed that the regression analyses do not account for a radial dependence of the independent variable (cf. Sec. II). Without a local correlation to the dependent variable, this radial dependence would essentially result in a larger uncertainty of the exponent. A finite correlation would affect the exponent, but a change in the scaling behavior is expected to originate from the turbulence characteristics in the first instance. Hence, it is here most important to note that the scaling behavior with the macroscopic parameter does not change

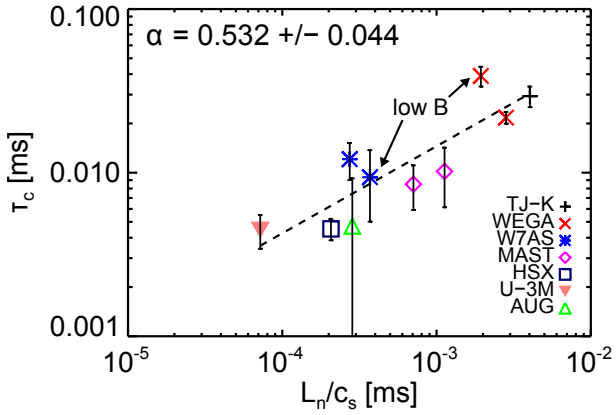

FIG. 7. Scaling of the correlation time τ_c (radial average) with the characteristic time scale L_n/c_s. The dashed line shows the best power law fit for $\tau_c \propto (L_n/c_s)^{\alpha}$.

substantially across the separatrix.

Similarly, the ρ_s scaling of L_c has been investigated, as displayed in Fig. 8. The AUG set was not taken into account for this scaling because data from a sufficient number of Langmuir probes is currently unavailable. With $\alpha = 0.55 \pm 0.04$, the exponent of the scaling relation is again below the expectation for pure drift-wave turbulence. To verify that the determined scaling relation is valid for the entire radial range, the sets were, as before, separated into the regions inside and outside the LCFS, yielding the following scaling exponents: $\alpha_{\mathrm{in}} = 0.52 \pm 0.04$ and $\alpha_{\mathrm{SOL}} = 0.54 \pm 0.05$. As for the τ_c scaling, all results are compatible within their uncertainties. Similar scaling exponents close to 0.5 were found in studies at TJ-K alone,[25] and agree with a prediction of the ρ_s-dependence for turbulence

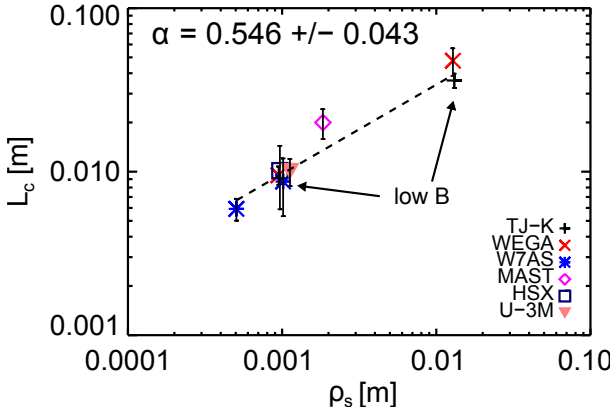

FIG. 8. Scaling of the correlation length L_c (radial average) with the drift scale ρ_s. The dashed line shows the best power law fit for $L_c \propto \rho_s^{\alpha}$.

with strong radial variation of profiles, $L_c \propto \sqrt{\rho_s L_n}$.[39]

Note that this scaling behavior corresponds to the detected dominant structure, which is certainly fed non-linearly by – but is not necessarily identical to – the most unstable mode. This could explain the difference to the linear ρ_s dependence of $1/k_{bend}$ in Sec. IV A. Furthermore, the scaling behavior of L_c with the macroscopic ρ_s suffers from an unresolved radial dependence in the same way as does that of τ_c (if at all). However, the agreement of the scalings in the inner edge and the SOL using local parameters has been confirmed in a very recent work by Fuchert et al.[40], which gives confidence that the radial T_e dependence is not crucial for the present scaling study.

With the weaker than linear dependencies of L_c and τ_c on ρ_s and L_n/c_s, respectively, a deviation from gyro-Bohm scaling could be expected for the turbulent diffusivity $D \propto L_c^2/\tau_c$. In fact, scaling analysis of D with the entire gyro-Bohm parameter $D_B\rho_s/L_n$ revealed a weaker power law with an approximate exponent of 0.5 inside as well as outside the LCFS. A complete list of scaling exponents is given in Table II.

TABLE II. Resulting scaling exponents for the turbulence properties τ_c, L_c and D.

Quantity	Scaling with	α overall	α inside	α SOL
τ_c	L_n/c_s	0.53 ± 0.04	0.60 ± 0.04	0.52 ± 0.04
L_c	ρ_s	0.55 ± 0.04	0.52 ± 0.04	0.54 ± 0.05
D	$D_B\rho_s/L_n$	0.50 ± 0.08	0.51 ± 0.07	0.50 ± 0.08

Even though the discharges in the ETDB are not strictly dimensionally similar, additional scaling investigations did not confirm any hidden dependence of the turbulence properties on the dimensionless collisionality ν^* or plasma beta β^*.

C. Conditional averaging results

The multi-machine database allows to test intermittent density events as general contributors to turbulent radial outward transport. Therefore, blobs and holes must be associated with outward and inward propagation, respectively. By identifying and averaging over intermittent spikes in the I_{sat} signal, the typical shape of density blobs or holes can be determined. At the same time, the Φ_{fl} measurements can be extracted whenever such a spike in the den-

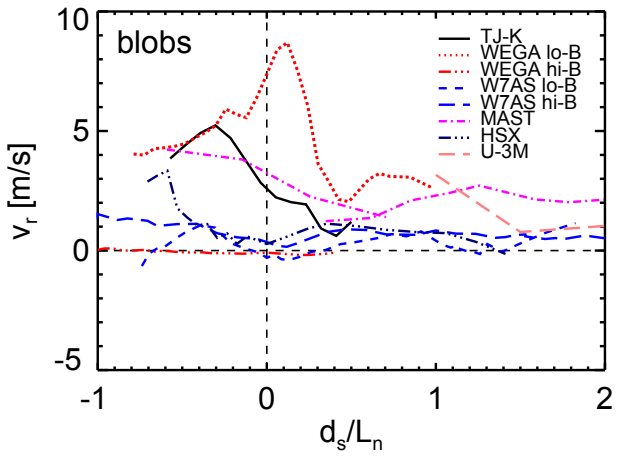

FIG. 9. Radial profile of v_r, as determined by conditional averaging. Results for positive peaks in $I_{\rm sat}$.

sity is detected. Since there are two measurements of the floating potential, the average electric field E_θ or radial velocity v_r can be calculated with the following approximation:

$$\tilde{E}_\theta \approx -\nabla\tilde{\Phi}_{\rm fl} \approx -\frac{\Delta\tilde{\Phi}_{\rm fl}}{d}, \qquad v_r = \frac{\tilde{E}_\theta}{B} \tag{5}$$

d is the distance between the probe tips measuring $\Phi_{\rm fl}$. Negative values of v_r correspond to inward motion.

Figures 9 and 10 show radial profiles of v_r during the detection of positive (blobs) and negative (holes) $I_{\rm sat}$ peaks, as obtained from the conditional averaging procedure. As has been well established from results of earlier works,[9,12,35] blobs are generally observed to propagate radially outwards. Hence, blobs contribute to outward particle transport across the LCFS and in the SOL of all ETDB devices. The behavior of holes is different. In some cases, v_r is directed inwards across the whole profile. Note that the inward motion of holes is also associated with outward transport. Outward-moving blobs and inward-moving holes are a symptom of a self-organized criticality system called the joint reflection symmetry.[41] For the TJ-K, MAST and low-B WEGA sets, v_r is positive inside and turns into negative values near the LCFS, before going back towards (or crossing) zero. The U-3M set might belong to the same group, but data inside the LCFS is not yet availabe. The outward radial motion of holes contributes to inward particle transport. For HSX, the radial velocity of holes points outward over the entire profile. Since the calculation of v_r requires data from two probe tips measuring $\Phi_{\rm fl}$ simultaneously, AUG data could not be included.

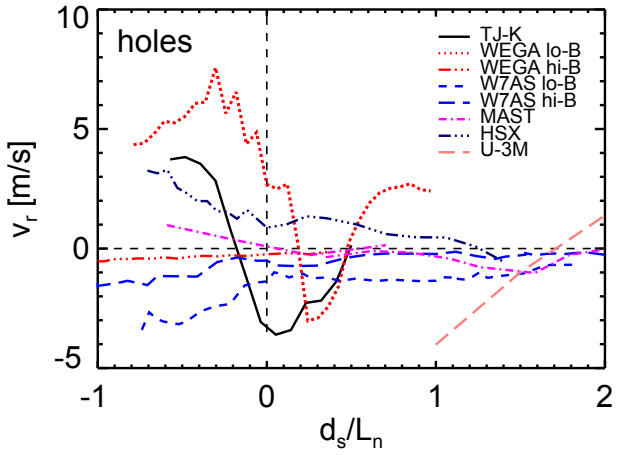

FIG. 10. Radial profile of v_r, as determined by conditional averaging. Results for negative peaks in $I_{\rm sat}$.

V. SUMMARY

This article presents analyses of plasma edge fluctuations measured with Langmuir probes at seven fusion research devices, collected in the international edge turbulence database. Typical turbulence power spectra with a dynamics over several orders of magnitude and nearly Gaussian probability distribution functions of the density fluctuatuions at the LCFS were characteristic for all datasets. The spectra show a bend at a frequency $f_{\rm bend}$ that scales approximately linearly with the characteristic device frequency $v_{\rm dia}/\rho_{\rm s}$. The product of the wavenumber at this bend and the drift scale, $k_{\rm bend}\rho_{\rm s}$, is approximately constant. Hence, as the injection range of a 2D turbulence spectrum, it shows the scaling behavior of linearly most unstable drift modes.

Radial profiles of the skewness confirmed the presence of blobs in the SOL of all devices, while in some sets, there are indications of holes inside the LCFS. The strong increase of the $I_{\rm sat}$ skewness with radius in the SOL can be explained by blobs which are propagating radially outward: as they pass through regions of quickly decreasing background density their own amplitude decreases slower and thus their influence on the skewness is increased.

For regions inside and outside the LCFS, scalings of correlation length $L_{\rm c}$ with the drift scale $\rho_{\rm s}$ and correlation time $\tau_{\rm c}$ with the characteristic timescale $L_n/c_{\rm s}$ were investigated separately. As independent variables in the regression analyses, macroscopic parameters deduced from quantities at the LCFS were used. In contradiction to expectations for drift-wave

turbulence (and particularly for most unstable drift modes), but consistent with previous results,[25] a square-root dependency was found for both:

$$L_\mathrm{c} \propto \sqrt{\rho_\mathrm{s}}, \qquad \tau_\mathrm{c} \propto \sqrt{\frac{L_n}{c_\mathrm{s}}} \tag{6}$$

The determined power law relations did not show significant variations between the edge of the confined plasma and the SOL, which points to a strong connection between turbulence in these regions. Although the scaling parameters under investigation lack radial resolution, the qualitative agreement with recent results in TJ-K[40] suggests that the use of macroscopic parameters for the presented scaling studies is justified. The general validity, however, needs to be verified in dedicated experiments resolving all parameters radially.

Furthermore, the turbulent diffusivity was estimated from the microscopic parameters. It was demonstrated to scale approximately with the square root of the gyro-Bohm coefficient, when the scalings from Eq. 6 are inserted:

$$D \propto \frac{L_\mathrm{c}^2}{\tau_\mathrm{c}} \propto \sqrt{D_\mathrm{B}\frac{\rho_\mathrm{s}}{L_n}} = \rho_\mathrm{s}\sqrt{\frac{c_\mathrm{s}}{L_n}} \propto \frac{1}{B} \tag{7}$$

Due to a different dependence on c_s and L_n, this scaling is neither exactly Bohm-like nor gyro-Bohm-like, falling in line with previous results from other devices.[42] But it is closer to a Bohm-like scaling when the dependence on the magnetic field is considered. In that regard, the results show reasonable agreement with the diffusivity scaling found at TJ-K[25]. It is important to note that the empirical scaling relations from Eqs. 6 and 7 are not dimensionally correct but rather only express the dependence on the parameters ρ_s and L_n/c_s that was confirmed in the analysis.

The influence of density blobs and holes on the radial transport was studied with a conditional averaging technique, confirming that blobs contribute to the radial particle transport in all devices while holes exhibit no consistent behavior. Consistent with the analysis of the skewness, in some cases, holes were observed to even create inward transport. The inward propagation of holes did not turn out to be a universal feature in the present analysis.

In summary, the edge turbulence database proved useful to investigate the characteristic features of plasma edge fluctuations. In the present set of devices, plasma blobs were recovered as a general contributor to transport in the SOL. Blobs, descended from drift waves inside the confinement region,[11] appear to also inherit characteristics such as the scaling

behavior, which for both drift waves and blobs indicates a weaker dependence of turbulent transport on the magnetic field strength than expected for a gyro-Bohm transport model.

ACKNOWLEDGMENTS

The author would like to thank the organisators of the International Stellarator-Heliotron Profile Database and the Coordinated Working Group for providing the framework for the ETDB. The ISHPDB is pursued under the auspices of the IEA Implementing Agreement for Cooperation in Development of the Stellarator Concept.

Financial support was given by the Directorate-General for Education and Culture of the European Commission under the Erasmus Mundus FUSION-EP program.

REFERENCES

[1]A. J. Wootton, B. A. Carreras, H. Matsumoto, K. McGuire, W. A. Peebles, Ch. P. Ritz, P. W. Terry, and S. J. Zweben, Phys. Fluids B 2, 2879 (1990)

[2]J. W. Connor, Plasma Phys. Control. Fusion 35, B293 (1993).

[3]J. W. Connor and H. R. Wilson, Plasma Phys. Control. Fusion 42, R1 (2000)

[4]P. W. Terry and P. H. Diamond, Phys. Fluids 28, 1419 (1985)

[5]B. Nold, S. Marsen, M. Ramisch, A. A. Beletskii, V. V. Chechkin, A. Dinklage, M. Endler, L. I. Grigor'eva, H. W. Müller, I. M. Pankratov, U. Stroth, P. Tamain, and R. Wilcox, Proceedings of the 37th EPS Conference on Plasma Physics, Dublin, 2010, edited by C. McKenna (Geneva, 2010), P1.1073.

[6]G. Y. Antar, P. Devynck, X. Garbet, and S. C. Luckhardt, Phys. Plasmas 8, 1612 (2001)

[7]J. A. Boedo, D. Rudakov, R. Moyer, S. Krasheninnikov, D. Whyte, G. McKee, G. Tynan, M. Schaffer, P. Stangeby, P. West, S. Allen, T. Evans, R. Fonck, E. Hollmann, A. Leonard, A. Mahdavi, G. Porter, M. Tillack, and G. Antar, Phys. Plasmas 8, 4826 (2001)

[8]J Bleuel, M Endler, H Niedermeyer, M Schubert, H Thomsen, and the W7-AS Team, New J. Phys. 4, 38 (2002)

[9]O. Grulke, J. L. Terry, B. LaBombard, and S. J. Zweben, Phys. Plasmas 13, 012306 (2006)

[10]A. Kirk, B. Koch, R. Scannell, H. R. Wilson, G. Counsell, J. Dowling, A. Herrmann, R. Martin, M. Walsh, and the MAST team, Phys. Rev. Lett. 96, 185001 (2006)

[11]T. Happel, F. Greiner, N. Mahdizadeh, B. Nold, M. Ramisch, and U. Stroth, Phys. Rev. Lett. 102, 255001 (2009)

[12]B. Nold, G. D. Conway, T. Happel, H. W. Müller, M. Ramisch, V. Rohde, U. Stroth, and the ASDEX Upgrade Team, Plasma Phys. Control. Fusion 52, 065005 (2010)

[13]S. J. Zweben, R. J. Maqueda, R. Hager, K. Hallatschek, S. M. Kaye, T. Munsat, F. M. Poli, A. L. Roquemore, Y. Sechrest, and D. P. Stotler, Phys. Plasmas 17, 102502 (2010)

[14]H. Y. W. Tsui, A. J. Wootton, J. D. Bell, R. D. Bengtson, D. Diebold, J. H. Harris, N. Hershkowitz, C. Hidalgo, J. C. Ingraham, G. X. Li, H. Lin, S. C. Luckhardt, D. M. Manos, M. A. Meier, G. M. Miller, C. P. Munson, J. Pew, Ch. P. Ritz, A. Rudyj, K. F. Schoenberg, J. Sorensen, T. Tanaka, T. Uckan, and P.G. Weber, J. Nucl. Mater. 196–198, 794 (1992)

[15]C. Hidalgo, Plasma Phys. Control. Fusion 37, A53 (1995)

[16]M. A. Pedrosa, C. Hidalgo, B. A. Carreras, R. Balbín, I. García-Cortés, D. Newman, B. van Milligen, E. Sánchez, J. Bleuel, M. Endler, S. Davies, and G. F. Matthews, Phys. Rev. Lett. 82, 3621 (1999)

[17]http://www.ipp.mpg.de/ISS/

[18]A. Kallenbach, V. Bobkov, F. Braun, A. Herrmann, H. Höhnle, R. M. McDermott, R. Neu, J.-M. Noterdaeme, T. Pütterich, J. Schweinzer, J. Stober, E. Strumberger, W. Suttrop, D. Wagner, and H. Zohm, IEEE Trans. Plasma Science 40, 605 (2012)

[19]M. Cox, and the MAST Team, Fusion Engineering and Design 46, 397 (1999)

[20]F. S. B. Anderson, A. F. Almagri, D. T. Anderson, P. G. Matthews, J. N. Talmadge, and J. L. Shohet, Fusion Technol. 27, 273 (1995)

[21]N. Krause, C. Lechte, J. Stöber, U. Stroth, E. Ascasibar, J. Alonso, and S. Niedner, Rev. Sci. Instrum. 73, 3474 (2002)

[22]V. V. Chechkin, I. M. Pankratov, L. I. Grigor'eva, A. A. Beletskii, A. A. Kasilov, P. Y. Burchenko, A. V. Lozin, S. A. Tsybenko, A. S. Slavnyj, A. P. Litvinov, A. Y. Kulaga, R. O. Pavlichenko, N. V. Zamanov, Y. K. Mironov, V. S. Romanov, V. K. Pashnev, S. M. Maznichenko, Y. D. Volkov, Probl. Atom. Sci. Tech. 82, 3 (2012)

[23]F. Wagner, S. Bäumel, J. Baldzuhn, N. Basse, R. Brakel, R. Burhenn, A. Dinklage, D. Dorst, H. Ehmler, M. Endler, V. Erckmann, Y. Feng, F. Gadelmeier, J. Geiger, L. Giannone, P. Grigull, H.-J. Hartfuss, D. Hartmann, D. Hildebrandt, M. Hirsch, E. Holzhauer, Y. Igitkhanov, R. Jänicke, M. Kick, A. Kislyakov, J. Kisslinger, T. Klinger, S. Klose, J. P. Knauer, R. König, G. Kühner, H. P. Laqua, H. Maassberg, K. McCormick, H. Nieder-

meyer, C. Nührenberg, E. Pasch, N. Ramasubramanian, N. Ruhs, N. Rust, E. Sallander, F. Sardei, M. Schubert, E. Speth, H. Thomsen, F. Volpe, A. Weller, A. Werner, H. Wobig, E. Würsching, M. Zarnstorff, and S. Zoletnik, Phys. Plasmas 12, 072509 (2005)

[24]M. Otte, H. P. Laqua, E. Chlechowitz, P. Drewelow, M. Glaubitz, S. Marsen, E. Müller, Y. Podoba, J. Schacht, T. Stange, F. Steffen, F. Wagner, R. Wolf, and D. Zhang, Contrib. Plasma Phys. 50, 780 (2010)

[25]M. Ramisch, N. Mahdizadeh, U. Stroth, F. Greiner, C. Lechte, and K. Rahbarnia, Phys. Plasmas 12, 032504 (2005)

[26]N. Mahdizadeh, F. Greiner, M. Ramisch, U. Stroth, W. Guttenfelder, C. Lechte, and K. Rahbarnia, Plasma Phys. Control. Fusion 47, 569 (2005)

[27]B. Nold, T. T. Ribeiro, M. Ramisch, Z. Huang, H. W. Müller, B. D. Scott, U. Stroth, and the ASDEX Upgrade Team, New J. Phys. 14, 063022 (2012)

[28]F. P. Gennrich and A. Kendl, Plasma Phys. Control. Fusion 54, 015012 (2012)

[29]M. Gilmore, W. A. Peebles, and X. V. Nguyen, Plasma Phys. Control. Fusion 42, L1 (2000)

[30]R. J. Adrian, Phys. Fluids 22, 2065 (1979)

[31]A. V. Filippas, Roger D. Bengston, G. X. Li, Mark Meier, Ch. P. Ritz, and E. J. Powers, Phys. Plasmas 2, 839 (1995)

[32]T. L. Rhodes, C. P. Ritz, and R. D. Bengtson, Nucl. Fusion 33, 1147 (1993)

[33]J. P. Graves, J. Horacek, R. A. Pitts, and K. I. Hopcraft, Plasma Phys. Control. Fusion 47, L1 (2005)

[34]O. E. Garcia, V. Naulin, A. H. Nielsen, and J. Juul Rasmussen, Phys. Plasmas 12, 062309 (2005)

[35]O. E. Garcia, J. Horacek, R. A. Pitts, A. H. Nielsen, W. Fundamenski, V. Naulin, and J. Juul Rasmussen, Nucl. Fusion 47, 667 (2007)

[36]O. E. Garcia, Plasma Fusion Res. 4, 019 (2009)

[37]U. Stroth, F. Greiner, C. Lechte, N. Mahdizadeh, K. Rahbarnia, and M. Ramisch, Phys. Plasmas 11, 2558 (2004)

[38]R. J. Goldston and P. H. Rutherford, *Introduction to Plasma Physics* (Institute of Physics Publishing, Bristol, 1995) p. 324

[39]N.A. Krall and M. N. Rosenbluth, Phys. Fluids 8, 1488 (1965)

[40]G. Fuchert, G. Birkenmeier, B. Nold, M. Ramisch, and U. Stroth, Plasma Phys. Control. Fusion 55, 125002 (2013)

[41]P. H. Diamond and T. S. Hahm, Phys. Plasmas 2, 3640 (1995)

[42]C. C. Petty, Phys. Plasmas 15, 080501 (2008)